K-shell ionization cross sections for Al, Ti, V, Cr, Fe, Ni, Cu, and Ag by protons and oxygen ions in the energy range 0.3—6.4 MeV

M. Geretschläger and O. Benka
Institut für Experimentalphysik, Johannes-Kepler-Universität Linz, A-4040 Linz, Austria
(Received 19 February 1986)

Absolute K-shell ionization cross sections have been measured for thin targets of Al, Ti, and Cu for protons in the energy range 0.3—2.0 MeV and for thin targets of Ti, V, Cr, Fe, Ni, Cu, and Ag for oxygen ions in the energy range 1.36—6.4 Mev. The experimental results are compared to the perturbed-stationary-state (PSS) approximation with energy-loss (E), Coulomb (C), and relativistic (R) corrections, i.e., the ECPSSR approximation (Brandt and Lapicki), to the semiclassical approximation (Laegsgaard, Andersen, and Lund), and to a theory for direct Coulomb ionization of the $1s\sigma$ molecular orbital [Montenegro and Sigaud (MS)]. The proton results agree within 3% with empirical reference cross sections. Also, the ECPSSR provides best overall agreement for protons. For oxygen ions, ECPSSR and MS predict experimental results satisfactorily for scaled velocities $\xi \geq 0.4$. For lower scaled velocities, the experimental cross sections become considerably higher than theoretical predictions for Coulomb ionization. This deviation increases with increasing Z_1/Z_2; it cannot be explained by electron transfer to the projectile or by ionization due to target recoil atoms.

I. INTRODUCTION

K-shell ionization by both light and heavy ions has been studied extensively in recent years. Various theoretical approaches with limited regions of validity have been used to predict total ionization cross sections. Madison and Merzbacher[1] classified the region of validity of ionization theories by the ratio of projectile and target charge (Z_1/Z_2) and by the ratio of projectile and target K-electron velocity (v_1/v_{2K}). The region of validity of molecular-orbital theory is characterized by $Z_1/Z_2 \sim 1$ and $v_1/v_{2K} \ll 1$. Theories for direct Coulomb ionization and for electron transfer are valid for $Z_1/Z_2 \ll 1$ and $v_1/v_{2K} \gtrsim 1$. The region of validity for direct Coulomb ionization has been extended to both less asymmetric and slower collisions by taking increased binding, Coulomb deflection, relativistic motion of target electrons, polarization of target atom by incident ion, and energy loss during collision into account. The aim of this work is to perform systematic studies of K-shell ionization for slow ($0.07 < v_1/v_{2K} < 0.18$) collisions, going from asymmetric ($Z_1/Z_2 = 0.17$) to less asymmetric ($Z_1/Z_2 \sim 0.36$) collisions, using oxygen ions. Although other authors (see Ref. 2) have measured cross sections in this range, our measurements go down to lower projectile energies. To check our procedure, we also measured cross sections for protons, where reliable data already exist (see Ref. 2).

II. EXPERIMENT

We used a 5 SDH Tandem accelerator manufactured by National Electrostatic Corporation to produce both protons of 0.3—2.0 MeV and oxygen ions of 1.3—6.4 MeV which had charge states of 1^+—3^+. The energy of the incoming particles was determined by means of an analyzing magnet which we calibrated with an accuracy of 0.2% in energy using the $^{19}F(p,\alpha\gamma)^{16}O$ resonances and the $^{27}Al(p,\gamma)^{28}Si$ resonance. The energy width of the ion beam was 1.8 keV full width at half maximum (FWHM). The ion beam was collimated by means of a stainless-steel aperture 1.5 mm in diameter mounted 8 cm from the target. The target currents were typically 10—150 particle nA.

We prepared our targets by vacuum evaporation of films of Al, Ti, V, Cr, Fe, Ni, Cu, and Ag onto polished slices of vitreous carbon. Table I shows the target thickness and the corresponding energy loss of oxygen ions from which this thickness was deduced. The angle between target surface vector and incoming ion beam was 30°. To prevent carbon contamination of our targets, we inserted a liquid nitrogen cold trap in our scattering chamber and maintained the pressure below 3.10^{-5} Pa.

The x-rays were measured using a Si(Li) detector at an angle of 150° with respect to the incoming ion beam. The energy resolution for the Mn $K\alpha$ line was 160 keV FWHM. The solid angle was defined by means of a stainless-steel aperture. We inserted absorber foils between target and detector in order to attenuate the L x-rays and to prevent backscattered energetic ions from

TABLE I. Target thickness (d) and energy loss (ΔE) of oxygen ions within the target for bombarding energies of 6 and 1.6 MeV, respectively. d is given in $\mu g/cm^2$ and ΔE is given in keV.

Target	ΔE_6	d_6	$\Delta E_{1.6}$	$d_{1.6}$
$_{22}$Ti	211	38	202	39
$_{23}$V	254	43	222	48
$_{24}$Cr	401	63	316	69
$_{26}$Fe	398	72	309	90
$_{28}$Ni	362	67	251	75
$_{29}$Cu	390	79	257	87
$_{47}$Ag	246	54		

reaching the detector. The foil absorption factors for the K x-rays of our targets were measured using 400-keV protons. The intrinsic detector efficiency was calculated from the detector window, the dead layer, and the detector thickness, as stated by the manufacturer, using the x-ray absorption cross sections from Veigele.[3]

A surface barrier detector was mounted at an angle of 156° with respect to the incoming beam for measuring the number of elastically backscattered ions and the energy loss of ions within our targets, respectively. The solid angle of the surface barrier detector was defined by means of a stainless-steel aperture. Since the energy-calibration curve of the surface barrier detector is rather nonlinear due to the energy-dependent energy loss of the ions in the detector window, we carefully determined this curve.

We measured simultaneously the x-ray spectra and the spectra of elastically scattered particles, using two analog-to-digital converters (ADC's). The counting rates were kept below 10^3 cps so that the pile-up-correction was smaller than 4%. Dead-time corrections were done electronically using the ADC busy signals. To evaluate the peak locations, the x-ray spectra were fitted[4] using Gaussian peak shapes and a linear background. The uncertainties of the peak energies thus determined were ± 3 and ± 10 eV for the $K\alpha$ lines and the $K\beta$ lines, respectively. The peak areas, however, were determined by simply summing all channels within a suitably chosen region in the x-ray spectra. Subsequently this number was multiplied by a background factor determined at high particle energy, since we found that the percentage of background was a fixed value for each element independent of ion energy. Using this technique we avoided, in cases of poor statistics, the additional large-peak-area errors introduced by individual background subtraction. The number of backscattered ions and the energy loss of ions within the target were determined using a fitting program,[5] which assumes a linear background due to plural scattering. Table II shows the estimated errors.

TABLE II. Sources of uncertainties in the measured x-ray cross sections.

(a) Individual systematical errors

x-rays:	Solid angle	6%
	Intrinsic efficiency	4–10 %
	Foil absorption	1%
Particles:	Solid angle	1%
	Backscatter angle	0.5%
	Bombarding energy	0.2%

(b) Total systematical errors

Al	Ti	V	Cr	Fe	Ni	Cu	Ag
10%	10%	13.5%	9.5%	9.5%	9.5%	9.5%	12%

(c) Nonsystematical errors

x-ray yield	0.3–12 %
Particle yield	0.3–3 %
Pileup and deadtime Correction	0.1–0.5 %
Energy loss within the target[a]	0.5–5 %

[a]The energy errors were converted to x-ray cross-section errors using theoretical cross sections for ionization (Ref. 9) and scattering (Ref. 6).

III. DETERMINATION OF EXPERIMENTAL X-RAY CROSS SECTIONS

If we bombard a target of thickness T having N atoms per unit volume with n ions of energy E_0 we will measure an experimental yield $Y^x_{\text{expt}}(E_0,T)$ according to Eq. (1),

$$Y^x_{\text{expt}}(E_0,T)=\epsilon^x nN\frac{\Omega^x}{4\pi}\times\int_0^T\sigma^x_{\text{expt}}[E(t)]\exp(-\mu\alpha t)dt\ . \quad (1)$$

Here σ^x_{expt} is the true x-ray production cross section which we want to extract from our yield measurements. ϵ^x is the intrinsic detector efficiency and Ω^x is the solid angle. The exponential corrects for target self-absorption; here μ is the x-ray absorption coefficient and the factor α depends on the angles between target normal, detector, and beam. $E(t)$ is the ion energy at depth t.

To correct for projectile energy loss within the target, we assume that we know a theoretical x-ray production cross section σ^x_{theor} which differs from the true σ^x_{expt} only by a constant (unknown) factor k. Then we have

$$\sigma^x_{\text{expt}}(E_0)=Y^x_{\text{expt}}(E_0,T)\times\sigma^x_{\text{theor}}(E_0)/Y^x_{\text{theor}}(E_0,T)\ , \quad (2)$$

where $Y^x_{\text{theor}}(E_0,T)$ is calculated replacing σ^x_{expt} by σ^x_{theor} in Eq. (1). To determine the product nN in Eq. (1) we measured also the yield of backscattered particles $Y^P_{\text{expt}}(E_0,T)$ as described above. Then we have

$$nN=Y^P_{\text{expt}}(E_0,T)\Big/\left[\Omega^P\int_0^T\frac{d\sigma^P[E(t)]}{d\Omega}dt\right]\ , \quad (3)$$

where $d\sigma^P/d\Omega$ is the particle backscattering cross section which is given exactly by theory and Ω^P is the solid angle of the particle detector. Combining Eqs. (1), (2), and (3) we have

$$\sigma^x_{\text{expt}}(E_0)=\frac{\Omega^P Y^x_{\text{expt}}(E_0,T)}{\Omega^x\epsilon^x Y^P_{\text{expt}}(E_0,T)}\times\frac{\sigma^x_{\text{theor}}(E_0)4\pi\int_0^T\{d\sigma^P[E(t)]/d\Omega\}dt}{\int_0^T\sigma^x_{\text{theor}}[E(t)]\exp(-\mu\alpha t)dt}\ . \quad (4)$$

Introducing the stopping power $S(E)=-dE/dt$, our evaluation prescription in the form actually used is

$$\sigma^x_{\text{expt}}(E_0)=\frac{\Omega^P Y^x_{\text{expt}}(E_0,T)}{\Omega^x\epsilon^x Y^P_{\text{expt}}(E_0,T)}\frac{\sigma^x_{\text{theor}}(E_0)4\pi\int_{E_1}^{E_0}\{[d\sigma^P(E)/d\Omega]/S(E)\}dE}{\int_{E_1}^{E_0}[\sigma^x_{\text{theor}}(E)/S(E)]\exp\left[-\mu\alpha\int_E^{E_0}dE'/S(E')\right]dE}\ , \quad (5)$$

TABLE III. Experimental x-ray production cross sections for oxygen ions on various targets given in barns. The integers in square brackets indicate powers of 10. Experimental errors are given in percent below the values. Errors are 10% except where stated. Calculated enhancement factors due to electron capture into the K' shell of the projectile (see text) are given in curly brackets except where they are less than 1.02. The charge state of incoming oxygen ions was 1+ for $E<2$ MeV and 3+ for $E>4$ MeV.

E (MeV)	$_{22}$Ti	$_{23}$V	$_{24}$Cr	$_{26}$Fe	$_{28}$Ni	$_{29}$Cu	$_{47}$Ag
6.40	1.41[+1] {1.13}					1.81 {1.03}	1.64[−2] (13%)
6.15	1.24[+1] {1.11}		5.56 {1.08}	3.30 {1.05}	1.86 {1.03}		
6.00	1.06[+1] {1.11}	7.76 {1.09} (14%)				1.37 {1.03}	
5.60	7.31 {1.10}					9.40[−1]	7.01[−3] (17%)
5.30	6.10 {1.08}		2.97 {1.06}	1.73 {1.03}	1.02 {1.02}		
5.20	5.51 {1.08}					7.63[−1] {1.02}	
4.80	3.91 {1.07}					5.60[−1]	
4.50	2.95 {1.06}					4.33[−1] {1.02}	
4.00	1.78 {1.05}		1.01 {1.03}	5.89[−1] {1.02}	3.17[−1] {1.02}	2.35[−1]	
3.70	1.25 {1.04}					1.58[−1]	
3.50	1.07 {1.03}		6.09[−1] {1.02}	3.42[−1]	1.70[−1]	1.17[−1]	
3.30	7.90[−1] {1.02}					8.95[−2]	
3.15	6.70[−1] {1.02}					6.77[−2]	
3.00	5.86[−1] {1.02}		3.25[−1]	1.58[−1]	8.01[−2]		
2.90	4.74[−1]					4.28[−2]	
2.70	3.62[−1]		2.04[−1]	9.32[−2]	4.34[−2]	2.86[−2]	
2.60		2.53[−1] (15%)					
2.50	2.43[−1]					1.78[−2] (11%)	
2.40	2.24[−1]		1.15[−1]	4.99[−2]	2.14[−2] (11%)		
2.30		1.39[−1] (15%)					
2.20	1.41[−1] (11%)					7.07[−3] (11%)	
2.10						6.01[−3] (14%)	
2.00	9.27[−2] (11%)		4.49[−2] (11%)	1.61[−2] (12%)	5.92[−3] (13%)		
1.90		5.16[−2] (17%)					
1.80	5.48[−2] (11%)		2.36[−2] (11%)	7.75[−3] (14%)	2.79[−3] (15%)		
1.70		2.59[−2] (18%)					
1.60	2.85[−2] (11%)		1.06[−2] (12%)	3.50[−3] (15%)	1.08[−3] (16%)	7.04[−4] (15%)	
1.50		1.31[−2] (18%)					
1.47	1.74[−2] (12%)		6.21[−3] (15%)	1.88[−3] (15%)			

TABLE III. (*Continued*).

E (MeV)	$_{22}$Ti	$_{23}$V	$_{24}$Cr	$_{26}$Fe	$_{28}$Ni	$_{29}$Cu	$_{47}$Ag
1.40	1.36[−2] (13%)	7.67[−3] (20%)					
1.36	1.26[−2] (13%)						

where E_1 is the ion energy at the last atomic layer of the target. The scattering cross section $d\sigma^P/d\Omega$ was corrected for atomic-screening effects following the prescription of Andersen *et al.*[6] The error of this cross section is believed[6] to be smaller than 1%. The proton stopping power was calculated following the procedure given by Andersen and Ziegler;[7] for oxygen ions, it was multiplied by the square of the effective charge which is given by Brandt and Kitagawa.[8] The absolute value of the stopping power does not contribute to errors in our evaluation since the stopping power serves only as weighting function and therefore only its relative accuracy within the integration limits is relevant. When we deduced the target thicknesses (Table I) from the energy loss of ions within the targets, as determined from the backscattering spectra, the apparent dependence of the target thickness on E_0 provided an estimate of the relative accuracy of the stopping power. We thus found that the stopping power contributes less than 0.5% to the error of σ^x_{expt}.

The theoretical x-ray production cross section $[\sigma^x_{\text{theor}}(E)]$ in Eq. (5) was calculated using Kropf's program[4] which calculates the perturbed-stationary-state approximation with energy-loss, Coulomb, and relativistic corrections (ECPSSR) ionization cross sections according to Brandt and Lapicki[9] (σ^I_{ECPSSR}, direct ionization only). The fluorescence yields ω were taken from Krause.[10] This theoretical x-ray production cross section, however, did not fulfill the assumption $\sigma^x_{\text{expt}}(E)=k\sigma^x_{\text{theor}}(E)$ with k being a constant independent of ion energy. Therefore an iterative procedure was necessary: From a first evaluation of our measurements we determined a correction function $C(E)$ for each target element by fitting a polynomial to the ratios $\sigma^x_{\text{expt}}(E_0)/\omega\sigma^I_{\text{ECPSSR}}(E_0)$. In the second step we replaced $\sigma^x_{\text{theor}}(E)$ in Eq. (5) by $\sigma^x_{\text{theor}}(E)=\omega C(E)\sigma^I_{\text{ECPSSR}}(E)$. A third step would have given no further improvement, hence our final results for oxygen ions (obtained in the second step) are given in Table III. We want to point out that our final result for σ^x_{expt} is independent of the chosen theoretical x-ray production cross section for the first step. The x-ray production cross sections given in Table III include all possible ionization mechanisms. Detailed discussions of individual contributions are given below. When we evaluated our proton cross sections, we found that k was independent of energy; hence no iteration was necessary. The proton results are given in Table IV.

TABLE IV. Experimental x-ray production cross sections for protons on various targets in units of barns. The integers in square brackets indicate powers of 10. Errors are given in percent below the values.

E (MeV)	$_{13}$Al	$_{22}$Ti	$_{29}$Cu
2.0			4.26[+1] (9.5%)
1.0	6.05[+2] (10%)	4.94[+1] (10%)	6.96 (9.5%)
0.6	3.00[+2] (10%)		
0.3	6.85[+1] (10%)		

IV. DISCUSSION

A. *K*-shell ionization by protons

We used the fluorescence yields of Krause[10] to convert our x-ray production cross sections to ionization cross sections. These were then compared to the empirical reference cross section σ_R given by Paul[2] and to the theoretical cross sections given by the following.

(a) Brandt and Lapicki,[9] who calculate plane-wave Born-approximation cross sections corrected for binding, polarization, energy loss during collision, Coulomb, and relativistic effects (σ_{ECPSSR}, direct ionization only),

(b) Laegsgaard, Andersen, and Lund,[11] who calculate semiclassical approximation cross sections corrected for binding, Coulomb, and relativistic effects (σ_{SCABCR}) and

(c) Montenegro and Sigaud (MS),[12] who apply adiabatic perturbation theory to the ionization of $1s\sigma$ molecular orbital by direct Coulomb interaction in asymmetric ion-atom collisions and extend the theory to less adiabatic collisions by imposing an asymptotic matching with the semiclassical approximation (σ_{MS}). In order to make comparisons to theory more convenient we show in Table V our experimental ionization cross sections (σ^I_{expt}) normalized to the reference cross sections[2] ($S_R=\sigma^I_{\text{expt}}/\sigma_R$), the ECPSSR cross sections[9] ($S_E=\sigma^I_{\text{expt}}/\sigma_{\text{ECPSSR}}$), the SCABCR cross sections[11] ($S_S=\sigma^I_{\text{expt}}/\sigma_{\text{SCABCR}}$), and the cross sections by Montenegro and Sigaud[12] ($S_M=\sigma^I_{\text{expt}}/\sigma_{\text{MS}}$), respectively. Proton energy is given in MeV and $\xi=2v_1/(\theta v_{2K})$ where v_1 is the lab projectile velocity, v_{2K} is the hydrogenic velocity of the target K-shell electron, and $\theta=I_K/(Z_2-0.3)^2R$ with I_K being the experimental ionization energy and R the Rydberg energy. As one can see from the values for S_R our experimental cross sections are in excellent agreement with values given in the literature.[2] The ECPSSR predictions[9] (direct ionization only) are accurate in the ξ range considered. The MS predictions[12] are slightly worse. The SCABCR theory[11] is much too low for large ξ, since its binding correction[13] is only good for $\xi<0.25$.

TABLE V. Experimental ionization cross sections for protons on various targets (Z_2) normalized to reference cross sections (S_R), ECPSSR cross sections (S_E), SCABCR cross sections (S_S), and $1s\sigma$-MO-Coulomb-ionization cross sections (S_M) (see text). Proton energy is given in MeV.

E	Z_2	ξ	S_R	S_E	S_S	S_M
2.0	29	0.78	1.01	0.98	0.99	1.00
1.0	29	0.55	0.99	0.96	0.86	0.92
1.0	22	0.75	0.98	0.95	0.96	0.94
1.0	13	1.40	0.97	0.99	1.53	1.10
0.6	13	1.09	0.99	0.98	1.34	1.07
0.3	13	0.77	1.02	0.99	1.08	0.96

B. *K*-shell ionization by oxygen ions

1. *Coulomb ionization*

K-shell ionization by all but the lightest ions is accompanied by simultaneous outer-shell ionization[1,14,15] which will increase the *K*-shell fluorescence yield. To estimate the magnitude of this effect we calculated the changes in fluorescence yields ($\delta\omega$) due to one additional *L*-shell vacancy following the proposition of Larkins[16] which is based on statistical scaling of x-ray and electron transition rates which are available from McGuire.[17] Assuming a linear dependence of fluorescence yield on the number of *L*-shell vacancies the corrected fluorescence yield becomes $\omega=\omega_0(1+n\delta\omega)$ where ω_0 is taken from Krause[10] and n is the number of *L*-shell vacancies. Using theoretical energy shifts of the K_α and K_β lines[18] the number of *L*-shell vacancies can be calculated from the measured energy shifts. For convenience we used the theoretical K_α and K_β x-ray energy shifts as a function of the number of $2p$ vacancies as given by Tanis *et al.*[19] The variation of ω thus obtained is small; the limiting values of ω and the corresponding experimental energy shifts ΔE for the K_α and K_β lines are given in Table VI.

Figures 1–3 show our experimental ionization cross sections (obtained using the corrected values of ω) normalized to theoretical predictions for Coulomb ionization, as a function of the logarithm of scaled velocity ξ. It is evident that in the lower ξ range experimental cross sections deviate strongly from all predictions for Coulomb ionization. In this ξ range the amount of deviation increases systematically with increasing Z_1/Z_2. Only for $\xi \gtrsim 0.4$ the ECPSSR predictions[9] (direct ionization only) and the MS predictions[12] are in rather good agreement with measurements. For the low projectile energies applied in this work measurements are not available in literature except one data point for 6-MeV oxygen ions on Ni given by Basbas *et al.*[20] which is in excellent agreement with our results. This data point is also shown in Figs. 1–3.

TABLE VI. Relative change of fluorescence yields and corresponding experimental energy shifts in eV for $K\alpha$ and $K\beta$ lines at the maximum and the minimum ion energy, respectively.

Target	$(\omega-\omega_0)/\omega_0$	ΔE_α	ΔE_β
$_{22}$Ti	0.06-0.01	20-3	83-42
$_{23}$V	0.05-0.01	22-4	90-38
$_{24}$Cr	0.04-0.01	24-9	93-37
$_{26}$Fe	0.04-0.01	30-13	99-45
$_{28}$Ni	0.04-0.01	39-9	115-43
$_{29}$Cu	0.03-0.01	29-8	97-45

2. *Electron capture*

The dependence of x-ray production cross sections on the charge state of the bombarding ions has been the subject of many investigations.[21–24] In cases where projectiles carried one or two *K*-shell holes, a significant cross-section enhancement was observed, but only small effects were found for projectiles with filled *K*-shell but different *L*-shell vacancy configurations. In this work the charge q_0 of incoming oxygen ions was always $q_0 \leq 3+$. But because of the low ion energies applied in this work we did not use vanishingly thin targets (see Table I) and hence we may have had charge states $q > q_0$ within our targets which might have enhanced the measured x-ray yield by *K*-to-*K* electron transfer. For 12-MeV oxygen ions on Ti and Cu, Knaf *et al.*[22] found target-thickness effects less than 20% when varying the thickness from 0.5 to 200 μg/cm^2. Considering that our highest oxygen energy is 6.4 MeV we feel that the x-ray production cross sections given in Table III do not differ by more than +10% from the x-ray production cross section for vanishingly thin targets.

Nevertheless, we want now to estimate more quantitatively the possible electron-transfer contribution to our

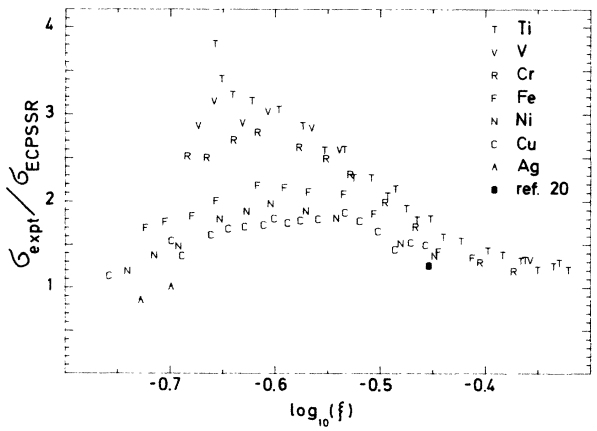

FIG. 1. Experimental ionization cross sections σ_{expt} normalized to ECPSSR cross sections (Ref. 9) (σ_{ECPSSR}).

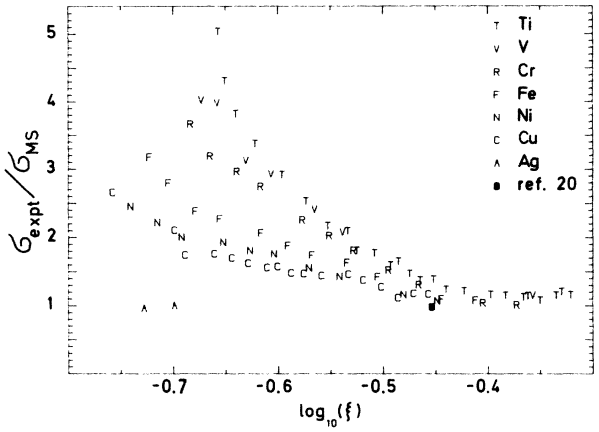

FIG. 2. Experimental ionization cross sections σ_{expt} normalized to the predictions of Montenegro and Sigaud (Ref. 12) (σ_{MS}).

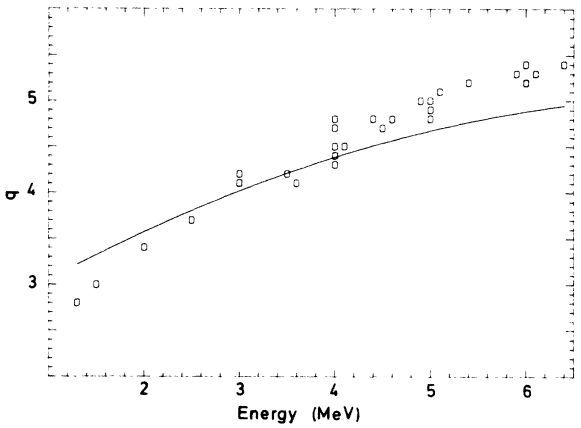

FIG. 4. Mean charge q of oxygen ions behind solids (Ref. 28). The solid line represents calculations according to Brandt and Kitagawan (Ref. 8).

measured cross sections. We assume that the total ionization is due to direct ionization (described by ECPSSR[9]) and to electron capture of target K electrons (K) into unoccupied electron states (S') of the moving ion described by the capture cross section ($\sigma_{KS'}$) of Lapicki and McDaniel.[25] The effective ionization cross section σ_{eff} of ions having a charge distribution of width d and mean charge q becomes

$$\sigma_{\text{eff}}(q,d)=\sigma_{\text{ECPSSR}}+w_{K'}(q,d)\sigma_{KK'}+w_{L'}(q,d)\sigma_{KL'}+w_{M'}(q,d)2\sigma_{KM'}\ , \tag{6}$$

where $w_{S'}(q,d)$ is the percentage of ions having an empty shell S' and the factor 2 takes care of contributions from higher shells $S'>M'$ (see Ref. 25). For vanishingly thin targets, we have, of course, $d=0$ and $q=q_0$. If the distribution of ion charge Q within the target is given by a smooth normalized function $f(Q,q,d)$ we have

$$w_{K'}(q,d)=\int_{Z_1-1/2}^{\infty} f(Q,q,d)dQ+0.5\int_{Z_1-3/2}^{Z_1-1/2} f(Q,q,d)dQ\ . \tag{7}$$

The fraction of ions having only one K hole is here weighted with a factor 0.5 since $\sigma_{KK'}$ holds for fully stripped ions. Similarly, one can calculate the fractions $w_{L'}(q,d)$ and $w_{M'}(q,d)$. Due to finite target thickness measured ionization cross sections are obviously enhanced by a factor $F=\sigma_{\text{eff}}(q,d)/\sigma_{\text{eff}}(q_0,0)$.

For the practical calculations based on Eq. (7) we used Gaussian distributions although it is known[26] that realistic charge-state distributions show high charge-state tails. Also the number of projectile K vacancies is believed[27] to be higher within the target, because of abundant excitation, than experimental charge distributions would suggest. We approximated the influence of both effects by using $d=0.54(Z_1)^{1/2}$ which is twice the value for the distribution width given by Betz.[26] Using experimental equilibrium charge-state distributions of oxygen ions behind solid targets[28] we determined values for the effective charge q for the energy range of interest which are given in Fig. 4 together with values calculated according to Ref. 8 (solid line). From a least-squares fit of a polynomial to those experimental values, we obtained the q values actually used in calculating $w_{K'}$ from Eq. (7). For the quantities $w_{L'}(q,d)$ and $w_{M'}(q,d)$ we simply chose uni-

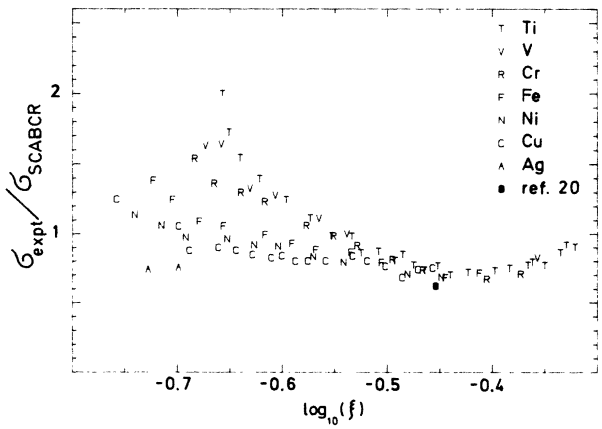

FIG. 3. Experimental ionization cross sections σ_{expt} normalized to SCABCR cross sections (Ref. 11) (σ_{SCABCR}).

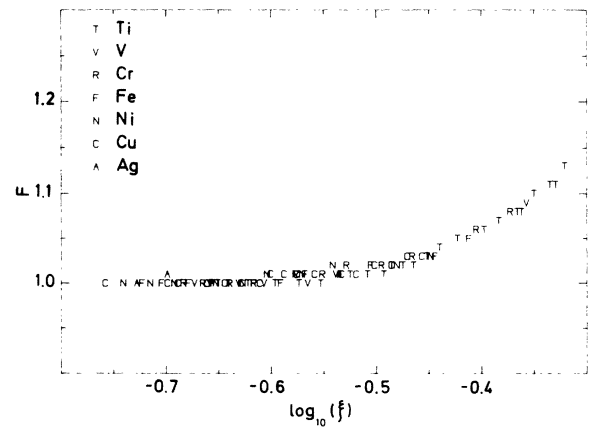

FIG. 5. Calculated enhancement factor F due to K-to-K'—shell electron capture for our targets.

ty. To prove the usefulness of our calculated enhancement factors we compared our results to experimental target-thickness effects in K—x-ray production for 52 MeV Si on Cu given by McDaniel *et al.*[29] and found reasonable agreement. The enhancement factors F due to K-to-K'—shell electron capture thus calculated are given in both Fig. 5 as a function of the logarithm of scaled velocity ξ and in Table III. It is evident that electron capture contributes significantly only at the highest ξ values. Taking the results given in Table III and Fig. 5 into account the agreement between experiment and theory would be even better for $\xi \gtrsim 0.4$ than indicated in Figs. 1 and 2. For totally stripped oxygen ions electron capture into shells higher than K' contributes less than 10% of the K-to-K' electron capture, and was therefore neglected.

3. MO ionization

For $Z_1/Z_2 \gtrsim 0.3$ and $v_1/v_{2K} \ll 1$ electron promotion between quasimolecular orbitals can contribute significantly to K-shell ionization.[30–32] Since the number of $2p\pi_x$ vacancies that are carried into the collision is not known, explicit calculations of ionization by the coupling of the inner $2p\sigma$ and $2p\pi_x$ orbitals are not possible. But a statistical treatment of the electron promotion from inner shells into the continuum has also been proposed[33–35] which makes the calculation of the sum of K-shell ionization cross sections of projectile and target atom straightforward. To determine the diffusion constant used in this model we took the formula of Brandt.[35] To deduce the individual K-shell ionization cross sections of both collision partners one can either use a vacancy-sharing formula of Meyerhoff *et al.*[36] or a semiempirical formula given by Stolterfoht *et al.*[37] Both give the same result within 30%. We used the semiempirical formula. For the lowest bombarding energies the target MO K-shell ionization cross sections, thus calculated, were lower than the experimental results by 3 orders of magnitude. But for those data points the vacancy-sharing ratio for the target K shell was of the order of 10^{-9} which is unrealistically low. It is known[37] that for $v_1/|Z_2-Z_1|<0.3$ the calculated sharing ratios drop off much too rapidly with decreasing velocity. Thus at those low bombarding energies MO cross sections can obviously not be calculated in this simple manner.

4. Contributions from recoiled target atoms

During the slowing-down process the oxygen ions produce recoil target atoms which, in turn, may ionize other target atoms. In a head-on collision a 1.6-MeV oxygen ion, e.g., would produce a 1.2-MeV Ti atom which would contribute very effectively to the emitted Ti x-ray yield since its MO-ionization cross section is considerably higher than the ionization cross section of 1.6-MeV oxygen ions on Ti. On the other hand, maximum energy transfer is rather improbable, so one cannot easily estimate the contribution of recoils. We therefore want to calculate the contribution of recoil atoms to the measured x-ray yield. If we bombard a target (Z_2,M_2) of thickness T with ions (Z_1,M_1) of energy $E_{1,0}$ these ions will, of course, be slowed down according to their stopping power $S_1(E)$, and will have energy E_1 at some depth t_1 and $E_{1,1}$ at depth T. The ions will also produce recoil atoms of energy $E_{2,0}$ which are scattered with a lab angle $\cos\Psi=[E_{2,0}(M_1+M_2)^2/4E_1M_1M_2]^{1/2}$ and which will have the energy $E_{2,1}$ according to their stopping power $S_2(E)$ when they leave the target. The contribution of one recoil target atom which is scattered at depth t_1 to the emitted x-ray yield is therefore given by

$$y_R^x(E_{2,0},E_1,t_1)=N\exp(-\mu\alpha_1 t_1)\times\int_{t_1}^{T}\sigma^x[E_2(t)]\exp(-\mu\alpha t)dt/\cos\Psi\ , \tag{8}$$

where N is the number of target atoms per unit volume, $\sigma^x[E_2(t)]$ is the x-ray production cross section of the recoil atoms, μ is the absorption coefficient, $\alpha_1=1/\cos\beta$ and $\alpha=\cos\Psi/\cos\beta$ with β being the angle between the target and the Si(Li) detector. Using the stopping powers $S_1(E)$ and $S_2(E)$, Eq. (8) becomes

$$y_R^x(E_{2,0},E_1)=N\exp\left[-\mu\alpha_1\int_{E_1}^{E_{1,0}}dE/S_1(E)\right]\times\int_{E_{2,1}}^{E_{2,0}}\exp\left[-\mu\alpha\int_{E_2}^{E_{2,0}}dE'/S_2(E')\right]\times\sigma^x(E_2)dE_2/S_2(E_2)\ . \tag{9}$$

The lower integration limit $E_{2,1}$ can be obtained from

$$\int_{E_{1,1}}^{E_1}dE/S_1(E)=\int_{E_{2,1}}^{E_{2,0}}\cos\Psi\,dE/S_2(E)\ . \tag{10}$$

Using the differential energy-transfer cross section $d\sigma[E_{2,0}(E_1)]$ we can now define the x-ray production cross section of recoil atoms $\sigma_R^x(E_1)$ which is given by

$$\sigma_R^x(E_1)=\int_0^{E_{2m}}y_R(E_{2,0},E_1)d\sigma[E_{2,0}(E_1)]\ , \tag{11}$$

where E_{2m} is the maximum energy transfer for ions with energy E_1. Taking now Eqs. (1) and (3) into account, the contribution of recoil atoms to the measured x-ray yield is

$$Y_R^x(E_{1,0},E_{1,1})=\frac{\epsilon^x\Omega^x}{4\pi\Omega^P}\frac{Y^P_{\text{expt}}(E_{10},E_{11})}{\int_{E_{1,1}}^{E_{1,0}}\frac{d\sigma^P(E_1)}{d\Omega S_1(E_1)}dE_1}\times\int_{E_{1,1}}^{E_{1,0}}\frac{\sigma_R^x(E_1)}{S_1(E_1)}dE_1\ . \tag{12}$$

For the practical calculations we used, in Eq. (9), the statistical MO-ionization cross section of Mittelman and Wilets.[33] The vacancy-sharing ratio was, of course, unity. In order to save computer time we calculated the function $S(w)$ (see Ref. 33) using $\log[S(w)]=f(\log w)$ where $f(\log w)$ is a polynomial of fourth order having the coefficients $A_0=-0.58117$, $A_1=0.85308$, $A_2=-1.2347$, $A_3=-0.55735$, and $A_4=0.60245$. From a comparison of MO cross sections thus calculated to experimental results[36] for Ar on Ar and Ni on Ni we found agreement within a factor of 5. Furthermore, we neglected target self-absorption and limited the lower integration limit

$E_{2,1}$ to 50 keV. We used fluorescence yields of Krause.[10] The stopping powers of the recoil atoms were calculated as described above. In Eq. (11) we used the screened energy-transfer cross section of Lindhard *et al.*[38] and the lower integration limit was fixed to 0.01 E_{2m}. The calculated x-ray yield of recoiled atoms was in all cases lower than 1% of the measured x-ray yield. Hence this effect cannot be responsible for the high cross sections found at low ξ.

VI. SUMMARY AND CONCLUSION

Measurements of ionization cross sections of protons on Al, Ti, and Cu and of oxygen ions on Ti, V, Cr, Fe, Ni, Cu, and Ag, respectively, were compared to theoretical predictions and to experimental results available in the literature (see Ref. 2). For protons an excellent agreement with both ECPSSR predictions[9] (direct ionization only) and reference cross sections[2] was found. For oxygen ions direct ionization was found to play a dominant role in target K vacancy production for values of scaled velocity $\xi \geq 0.4$ where ECPSSR theory[9] and $1s\sigma$-MO-Coulomb-ionization predictions[12] are in good agreement with experimental results. Because of finite target thickness electron capture may contribute in this ξ range up to 10% of the measured vacancy production. For values $\xi < 0.3$, however, electron capture contributes practically nothing, but the measured ionization cross sections were substantially higher than the predictions of direct-ionization theories and this deviation increases with increasing Z_1/Z_2. Similar (but smaller) deviations of σ_{expt} for oxygen projectiles from σ_{ECPSSR} have been found by Paul[2] for smaller values of Z_1/Z_2 (i.e., heavier targets). Knaf *et al.*[22,39] obtained deviations of a magnitude similar to that shown in our Fig. 1 when measuring the cross sections for 2–28-MeV fluorine ions on various targets (although this cannot be seen so clearly from their graphs). It could be[2] that a better description of the binding correction is sufficient, or that electron promotions within the molecular orbital model are necessary to describe the experimental data properly. Contributions of recoil target atoms to K-shell ionization were found to be negligible.

ACKNOWLEDGMENTS

We would like to thank Professor Helmut Paul for calculating the reference cross sections and for many helpful discussions. This work was partially supported by the "Fonds zur Förderung der wissenschaftlichen Forschung," Project No. 4303.

[1]D. H. Madison and E. Merzbacher, in *Atomic Inner Shell Processes*, edited by B. Crasemann (Academic, New York, 1975).
[2]H. Paul and J. Muhr, Phys. Rep. **135**, 47 (1986).
[3]W. M. Veigele, At. Data Nucl. Data Tables **5**, 51 (1979).
[4]A. Kropf, Diploma Thesis, University of Linz, 1982.
[5]D. Semrad and P. Bauer, Nucl. Instrum. Meth. **149**, 159 (1978).
[6]H. H. Andersen, F. Besenbacher, P. Loftager, and W. Möller, Phys. Rev. A **21**, 1891 (1980).
[7]H. H. Andersen and J. F. Ziegler, *Hydrogen Stopping Powers and Ranges in all Elements* (Pergamon, New York, 1977).
[8]W. Brandt and M. Kitagawa, Phys. Rev. B **25**, 5631 (1982).
[9]W. Brandt and G. Lapicki, Phys. Rev. A **23**, 1717 (1981).
[10]M. O. Krause, J. Phys. Chem. Ref. Data **8**, 307 (1979).
[11]E. Laegsgaard, U. J. Andersen, and M. Lund, *Proceedings of the Tenth International Conference on Physics of Electron and Atomic Collisions, Paris, 1977*, edited by G. Watel (North-Holland, Amsterdam, 1977).
[12]E. C. Montenegro and G. M. Sigaud, J. Phys. B **18**, 299 (1985).
[13]H. Paul, Nucl. Instrum. Meth. **169**, 249 (1980).
[14]D. Burch and P. Richard, Phys. Rev. Lett. **25**, 983 (1970).
[15]J. D. Garcia, J. R. Fortner, and T. M. Kavanagh, Rev. Mod. Phys. **45**, 111 (1973).
[16]F. P. Larkins, J. Phys. B **4**, L29 (1971).
[17]E. J. McGuire, Phys. Rev. A **2**, 273 (1970).
[18]F. Hermann and S. Skillmann, *Atomic Structure Calculations* (Prentice-Hall, Englewood Cliffs, 1963).
[19]J. A. Tanis, S. M. Shafroth, W. W. Jacobs, T. McAbee, and G. Lapicki, Phys. Rev. A **31**, 750 (1985).
[20]G. Basbas, W. Brandt, and R. Laubert, Phys. Rev. A **17**, 1655 (1978).
[21]T. J. Gray, in *Methods of Experimental Physics* (Academic, New York, 1980), Vol. 17, p. 250.
[22]B. Knaf, G. Presser, and J. Stähler, Z. Phys. A **282**, 25 (1977).
[23]G. Presser, E. Scherer, and J. Stähler, Z. Phys. A **295**, 27 (1980).
[24]H. Tawara, P. Richard, T. J. Gray, P. Pepmiller, J. R. Macdonald, and R. Dillingham, Phys. Rev. A **19**, 2131 (1979).
[25]G. Lapicki and F. D. McDaniel, Phys. Rev. A **22**, 1896 (1980).
[26]H. D. Betz, Rev. Mod. Phys. **44**, 465 (1972).
[27]H. D. Betz, private communication.
[28]A. B. Wittkower and H. D. Betz, At. Data **5**, 113 (1973).
[29]F. D. McDaniel, J. L. Duggan, G. Basbas, P. D. Miller, and G. Lapicki, Phys. Rev. A **16**, 1375 (1977).
[30]U. Fano and W. Lichten, Phys. Rev. Lett. **14**, 627 (1963).
[31]K. Taulbjerg, J. S. Briggs, and J. Vaaben, J. Phys. B **9**, 1351 (1976).
[32]W. E. Meyerhof and K. Taulbjerg, Annu. Rev. Nucl. Sci. **27**, 279 (1977).
[33]M. H. Mittelman and L. Wilets, Phys. Rev. **154**, 12 (1967).
[34]W. Brandt and K. W. Jones, Phys. Lett. **57A**, 35 (1976).
[35]W. Brandt, IEEE Trans. Nucl. Sci. **NS-26**, 1179 (1979).
[36]W. E. Meyerhof, R. Anholt, and T. K. Saylor, Phys. Rev. A **16**, 169 (1977).
[37]N. Stolterfoht, P. Ziem, and D. Ridder, J. Phys. B **7**, L409 (1974).
[38]J. Lindhard, Vibeke Nielsen, and M. Scharff, K. Dan. Vidensk. Selsk. Mat.-Fys. Medd. **36**, 10 (1968).
[39]B. Knaf, G. Presser, and J. Stähler, Z. Phys. A **289**, 131 (1979).